pubs.acs.org/Biomac

Article

Helical Peptoid Ions in the Gas Phase: Thwarting the Charge Solvation Effect by H-Bond Compensation

Sébastien Hoyas, Perrine Weber, Emilie Halin, Olivier Coulembier, Julien De Winter, Jérôme Cornil,* and Pascal Gerbaux*

Cite This: *Biomacromolecules* 2021, 22, 3543−3551

Read Online

ACCESS | Metrics & More | Article Recommendations | Supporting Information

ABSTRACT: Folding and unfolding processes are key aspects that should be mastered for the design of foldamer molecules for targeted applications. In contrast to the solution phase, in vacuo conditions represent a well-defined environment to analyze the intramolecular interactions that largely control the folding/unfolding dynamics. Ion mobility mass spectrometry coupled to theoretical modeling represents an efficient method to decipher the spatial structures of gaseous ions, including foldamers. However, charge solvation typically compacts the ion structure in the absence of strong stabilizing secondary interactions. This is the case in peptoids that are synthetic peptide regioisomers whose side chains are connected to the nitrogen atoms of the backbone instead of α-carbon as in peptides, thus implying the absence of H-bonds among the core units of the backbone. A recent work indeed reported that helical peptoids based on *N*spe units formed in solution do not retain their secondary structure when transferred to the gas phase upon electrospray ionization (ESI). In this context, we demonstrate here that the helical structure of peptoids bearing (*S*)-*N*-(1-carboxy-2-phenylethyl) bulky side chains (*N*scp) is largely preserved in the gas phase by the creation of a hydrogen bond network, induced by the presence of carboxylic moieties, that compensates for the charge solvation process.

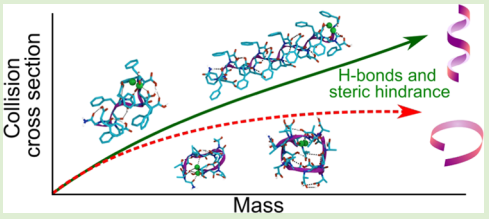

1. INTRODUCTION

Over the years, non-natural compounds able to dynamically fold and unfold into well-defined secondary structures called "foldamers" have aroused interest in many fields.[1−3] Several different biomimetic compounds are part of this class, such as β- and γ-peptides,[4] oligoureas,[5] and peptoids.[6] The later, built from N-substituted glycines, are peptidomimetic molecules, whose backbone lacks amide hydrogen bond donor and chirality (Scheme 1).[7] One of the main advantages of these non-natural molecules is the availability of a wide variety of building blocks, especially for peptoids,[8] which enables new structural design compared to existing molecules for applications. Another advantage of peptoids is their high resistance to protease as well as to harsh conditions,[9,10] which makes them good candidates to replace antimicrobial peptides.[3,11] Peptoids are not only used in biomedical fields[12,13] but also in molecular recognition processes,[14] as bulk materials,[15,16] and in nanotechnology.[14,17] The most common type of structure encountered is the helical shape,[11,18,19] which is the most adequate way to form a tightly packed secondary structure.[20] Peptoids can form helices in solution, provided that the side chain appended to the nitrogen is bulky and chiral, to induce a particular screw sense.[19,21] Such structures are mainly stabilized by noncovalent interactions, such as $n \rightarrow \pi^*$ interactions between adjacent amides,[22] which can be however altered by solvent. Therefore, in vacuo studies are also of great interest to provide a deeper insight into the intrinsic parameters responsible for the folding of foldamers and lead to new molecular design strategies.[23−25] Ion mobility spectrometry coupled to mass spectrometry (IMS-MS) is one of the most relevant tools to characterize the conformational dynamics and folding in vacuo.[26−28] This technique allows for

Scheme 1. Primary Structures of Peptides and Peptoids and of the Side Chains Studied (*n* Varying from 3 up to 15)

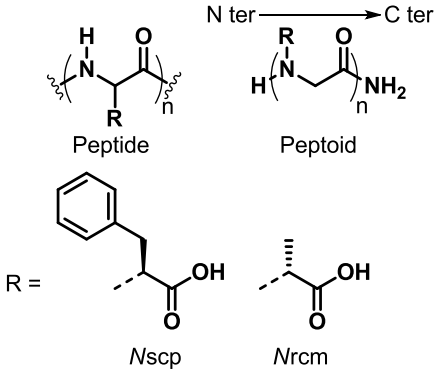

Received: May 18, 2021
Revised: July 1, 2021
Published: July 12, 2021

https://doi.org/10.1021/acs.biomac.1c00623
Biomacromolecules 2021, 22, 3543−3551

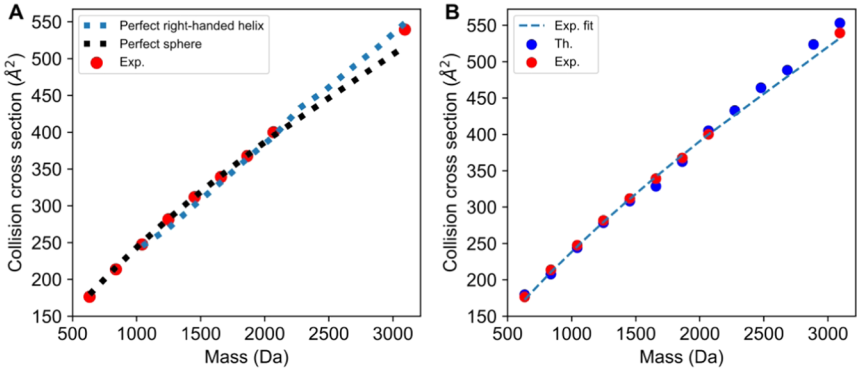

Figure 1. Experimental and theoretical collision cross sections (CCS) of singly protonated *N*scp peptoids. (A) Comparison of the size evolution of the experimental $^{TW}\Omega_{N_2\rightarrow He}$ (red dots) with the values predicted for perfectly spherical (black dashed line) and helical (blue dashed line) ions (see text). (B) Comparison of the experimental $^{TW}\Omega_{N_2\rightarrow He}$ (red dots) with the theoretical Ω_{He} values calculated on structures generated by MD simulations (blue dots). The experimental data are further fitted (blue dashed line) by the expression $\Omega = AM^B$, with A = 1.77 and B = 0.71 (see text).

the separation of ions in the gas phase according to their mass-to-charge ratio (m/z) and their tridimensional shape. It is widely exploited with peptides/proteins, as it allows the determination of the protein conformation by measuring their collision cross sections (Ω).[29,30] Additionally, IMS-MS has also been applied to polymer chains; one illustrative example is the use of ion mobility to distinguish isomeric structures, such as linear versus cyclic species.[31,32] IMS-MS has also been involved in the study of Hudgins et al. to shed light on the formation of α-helices built from amino acids.[33] They showed that poly(alanine) peptides can remain helical in the gas phase, provided that the positive charge introduced for ionization (proton) is present at the negative side of the macrodipole (C-terminus).[23] Although peptoids are structurally close to peptides, we recently reported that peptoid ions bearing bulky chiral (*S*)-*N*-(1-phenylethyl) side chains (*N*spe) do not form helices in the gas phase (although helices are evidenced in solution) but rather loop-like structures to stabilize the introduced charge, mandatory for IMS-MS analysis.[34] The steric hindrance responsible for the folding of peptoids is thus not sufficient to compensate for the charge screening effect.[33,35] In the present work, we have introduced hydrogen bonding donor/acceptor pairs through the incorporation of the peptoid side chain "(*S*)-*N*-(1-carboxy-2-phenylethyl)" (*N*scp) all along the peptoid backbone.[36] Our objective is to study the impact of these intramolecular hydrogen bonds on the structure of the gas phase ions by combining ion mobility mass spectrometry measurements with molecular dynamics simulations. The influence of the side chain bulkiness on the stabilization of particular structures has also been monitored at the theoretical level using the "(*R*)-*N*-(1-carboxy-2-ethyl)" (*N*rce) side chain.

2. EXPERIMENTAL SECTION

2.1. Peptoid Synthesis. All reactants and solvents are commercially available (VWR chemicals) and are used without any supplementary purification. *N*scp peptoids are synthesized by successive acylation and nucleophilic substitution steps on Rink amide resin using the solid-phase reaction protocol developed by Zuckermann and co-workers: all details are described elsewhere.[8,37] The primary amine required to incorporate the *N*scp side chain during the nucleophilic substitution is previously prepared from L-phenylalanine by esterification to protect the carboxylic groups. At 0 °C, thionyl chloride (11 ml, 0.15 mol) is slowly added into methanol (150 mL). L-Phenylalanine is then added at room temperature and the solution is stirred for 48 h. After the synthesis of $Nscp_{3-9}$ sequences, the carboxylic groups can be deprotected by hydrolysis with 5 M NaOH (3 mL) and methanol (4 mL) to 55 °C for 5 h. $Nscp_{10}$ and $Nscp_{15}$ require overnight hydrolysis to recover the carboxylic moieties. *N*scp peptoids are prepared without further purification since they are only analyzed by mass spectrometry, which isolates the targeted ions in the gas phase. The structure of the peptoids is validated using collision-induced dissociation experiments (Table S1).

2.2. Ion Mobility Experiments. Ion mobility spectrometry measurements are performed using a Synapt G2-S*i* (Waters, U.K.) mass spectrometer equipped with an electrospray (ESI) ionization source and a traveling wave ion mobility cell pressured with N_2 as the drift gas. The IMS parameters and the sample preparation are described in the Supporting Information. In TWIMS experiments, calibration is required to convert the measured drift times in nitrogen into collision cross sections in helium ($^{TW}\Omega_{N_2\rightarrow He}$).[38] The calibrants used in these experiments are polymer ions (poly(ethylene glycol)—PEG and α-methyl, ω-hydroxy polylactide—PLA).[34,39] The analyses are performed in different solvents (acetonitrile and methanol/acetonitrile 1:1 v/v). The collision cross sections Ω are abbreviated using the current accepted notation;[28] $^{TW}\Omega_{N_2\rightarrow He}$ refers to the experimental collision cross sections and Ω_{He} to the theoretical collision cross sections (TM stands for the trajectory method).

2.3. Computational Chemistry. Simulations are performed within the Materials Studio 18.0 package using the PEPDROID force field,[40] based on the DREIDING force field, in conjunction with Gasteiger partial charges.[41−43] Many different side chain parameters are already implemented in this force field, but not for the side chains *N*scp and *N*rce under investigation (Scheme 1). To do so, we follow the same procedure as described in the original paper.[41] Briefly, we perform an energy scan of the dihedrals for a small peptoid unit (ω, χ_1, and χ_2 in Scheme S1) at a quantum-mechanical level (MP2/cc-pVDZ) using the Gaussian09 package revision A02.[44] We then perform the same scan at the MM level in Materials Studio 18.0, and the dihedral parameters are systematically adapted to yield the lowest RMSD between the QM and MM energy profiles. A complete description is available in the Supporting Information (Figures S1 and S2).

After the validation of the parameters, multiple starting geometries are generated for each degree of polymerization (DP), i.e., in the right-handed helical shape and in multiple random conformations (collapsed, extended, etc.). Each of them is first optimized and then submitted to a conformational search, which is described in ref 34. Briefly, multiple consecutive quenched molecular dynamics (quenched MD) are performed at different temperatures on each starting geometry to sample their conformational space (NVT, 1000

https://doi.org/10.1021/acs.biomac.1c00623
Biomacromolecules 2021, 22, 3543−3551

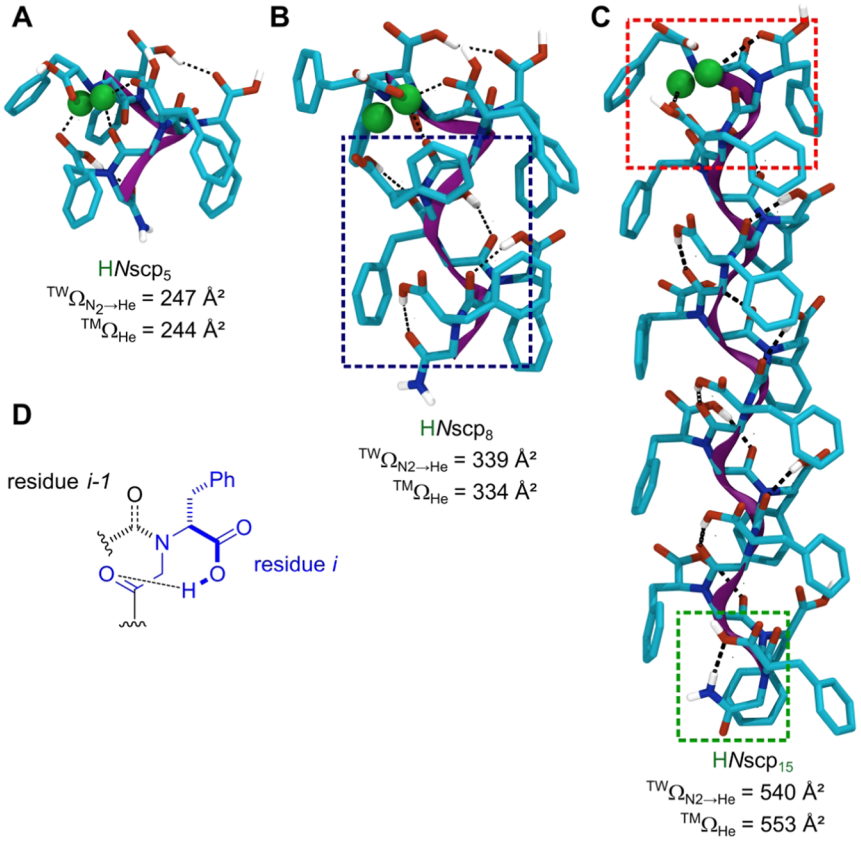

Figure 2. Most stable structures of different *N*scp peptoid ions generated during the conformational sampling. Hydrogen bonds are represented by black dashed lines and only relevant hydrogen atoms are represented. The hydrogen atoms of the ammonium groups are represented by green balls. For low polymerization degrees (A), the backbone almost completely wraps around the proton, while for higher polymerization degrees, (B) and (C), the first units around the terminal amine are involved in the stabilization of the proton, and the remaining part starts organizing in a helical fashion through a hydrogen bond network (blue dot box). (D) Schematic of the intraresidue hydrogen bond pattern.

K down to 200 K, 20 ns, frame saved every 5 ps). The most stable conformation issued from a quenched MD is set as input for the next quenched MD at a lower temperature. The final geometry selected is the most stable among the multiple conformations generated for a given DP at the end of the quenched dynamics. A final equilibration MD (NVT, 300 K, 10 ns) is carried out on the selected structure and is followed by a production MD for 50 ns. The collision cross section Ω_{He} calculation is carried out using Collidoscope software.[45] Five hundred conformations (saved every 0.1 ns) are extracted from the production run and submitted to Collidoscope to first estimate the cross section with the trajectory method and come up with average values.

3. RESULTS AND DISCUSSION

3.1. (*S*)-*N*-(1-Carboxy-2-phenylethyl) (*N*scp) Peptoids. The *N*scp$_n$ (n = 3−15) peptoids under investigation carry a proton at the N-terminus amine, which is the most basic site.[34,46] Singly charged peptoids (protonated) are transferred to the gas phase by ESI. They are then transferred to the mobility cell and their arrival time distribution (ATD) is recorded and converted into $^{TW}\Omega_{N_2\rightarrow He}$ through the in-house calibration procedure.[39] The CCS distributions are presented in the Supporting Information for evaluating the presence of different non-interconverting ion structures, based on the symmetry of the signals. As shown in Figure S8, the CCS signals all present a Gaussian shape and the ion mobility resolution is only marginally affected by the chain length increase. However, due to the rather limited IM resolution of the Waters Synapt G2-S*i* mass spectrometer, the coexistence of different ion structures with similar CCS cannot be excluded.[47] We report in Figure 1A the $^{TW}\Omega_{N_2\rightarrow He}$ as a function of ion mass for each degree of polymerization (DP). A general procedure to analyze series of homologous compounds is to fit the data by a power law of the form $\Omega = AM^B$, where M is the molecular mass, B is a parameter that reflects the general shape of the ions, and A reflects the ion density.[34,38,48] For ions that adopt a globular shape in the gas phase (proteins, polymers), parameter B is determined to be around 2/3 (0.66), while parameter A is on average equal to 2.435.[39,48,49] In the present study, we obtain a parameter B of 0.71 and a parameter A of 1.77 (Figure 1B, blue dashed curve), indicating that these ions are less compact than globular ions. In a previous study dedicated to *N*spe peptoid ions, parameter B was estimated at 0.685, pointing to more compact structures in comparison to the present derivatives.[34] Interestingly, the DP 3−8 ions are perfectly aligned on the fitting curve, while the higher DP ions lie a bit off, as there is a small hinge in the curve. When isolating the data for the smaller range from 3 to 8, we obtain B = 0.68 and A = 2.18, which are parameters characteristic of a globular shape, thus implying that these ions are more compact than suggested by the fit performed on the entire data set. For the DP 9−15 range, we obtain B = 0.74 and A = 1.36, which evidences a structuring into more extended conformers. As a matter of comparison, we have added in Figure 1A the chain size evolution of the collision cross sections associated with the parameters of perfectly spherical ions (B = 0.66 and A = 2.435; Figure 1A, black dotted curve). From the graphs, we clearly

https://doi.org/10.1021/acs.biomac.1c00623
Biomacromolecules 2021, 22, 3543−3551

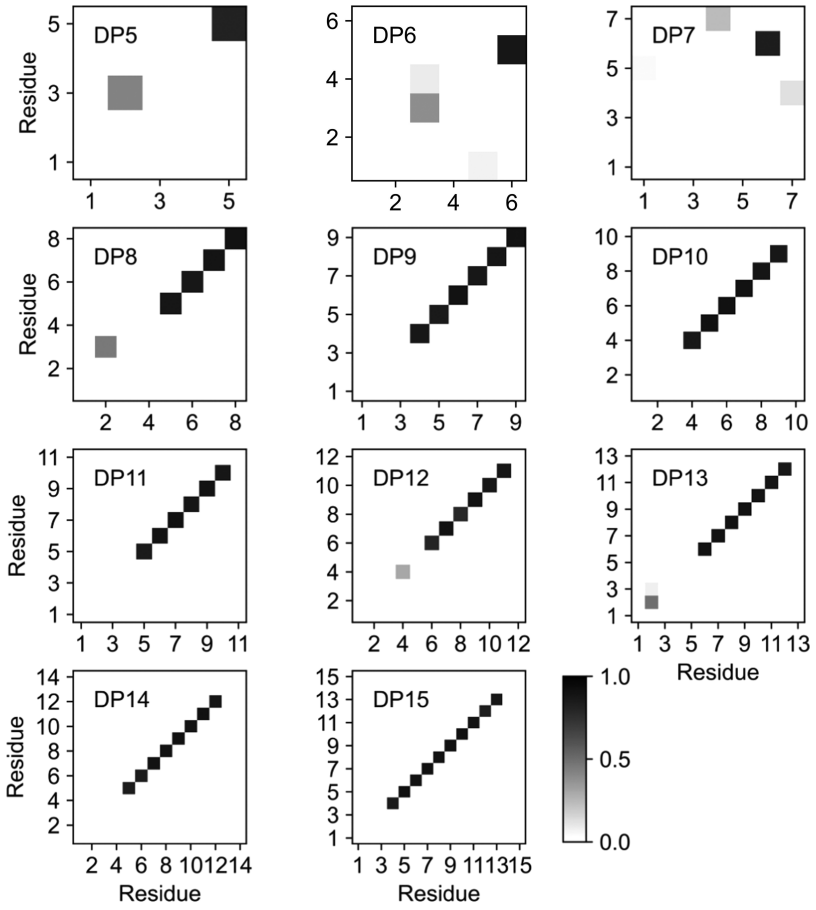

Figure 3. Hydrogen bond correlation matrices for *N*scp peptoids ranging from DP 5 to 15 along 50 ns MD simulations. The *X*- and *Y*-axes correspond to the residue number starting from the N-terminus. The hydrogen bonds are monitored simultaneously between the hydrogen of the carboxylic acid moieties (donor) and the oxygen from (i) the carbonyls of the backbone and (ii) the carbonyls of the carboxylic functions (acceptor) The cutoff distance between the donor and the acceptor is set at 3.5 Å and the cutoff angle at 150°.[50] Black squares represent robust H-bonds along the MD, while lighter colors indicate that the H-bonds are more labile. The diagonal pattern observed for a DP higher than 8−9 units indicates the conservation of the intramolecular hydrogen bonds with the carbonyl group from the amide of the same residue over the whole simulation.

observe that the $^{TW}\Omega_{N_2\rightarrow He}$ values of the low DP ions are in really good agreement with trends predicted for spherical shape ions and they start deviating for higher DP ions (higher mass). Since the more extended structure might correspond to a helix, we built perfectly helical peptoid ions for each DP (from 5 to 15), with a screw sense determined by the chirality of the side chain (here, (*S*), right-handed), using the same dihedrals as described in ref 34. These conformers were not submitted to any MD simulation to maintain the ideal helix structure. Their Ω_{He} values are computed, and the evolution as a function of mass is represented in Figure 1A as a light blue dotted curve. The experimental DP 9−15 CCS align very well on the curve predicted for a helix, further demonstrating that higher DP ions adopt extended structures that are most likely helical.

To further validate the hypothesis that *N*scp peptoid ions start to adopt more extended helical conformations when their length reaches about 8−9 units, we perform MD simulations on peptoid ions with DP ranging from 3 to 15. As discussed above, peptoids are protonated on the terminal amine in the gas phase, which is the most basic site accessible.[34] The more stable structures obtained after conformational sampling for *N*scp$_5$, *N*scp$_8$, and *N*scp$_{10}$ are presented in Figure 2 as selected examples. The Ω_{He} associated with the most stable conformation of each DP is in good agreement with the $^{TW}\Omega_{N_2\rightarrow He}$ experimental data. The conformations adopted by shorter oligomers, i.e., *N*scp$_n$ with n = 3−5, are similar to those of short *N*spe peptoid ions, with the peptoid backbone wrapping around the charge.[34] As shown in Figure 2A, all carbonyl dipoles point toward the charged site to induce charge solvation.[34] In contrast, the most stable conformations for longer oligomers, i.e., *N*scp$_8$ and *N*scp$_{15}$, appear more extended with the appearance of a right-handed helix organization at the C-terminus extremity (Figure 2B). Although the first three/four residues lying at the N-terminus side of the peptoid ion remain strongly bounded to the ammonium group, the remaining residues get organized into a helix-like structure, thanks to the creation of a mostly intraresidue hydrogen bond network, as shown in Figure 2C for DP 15.

We also analyze whether these intraresidue H-bonds are stable during the MD simulations. For each peptoid chain length (n = 5−15) and for all structures generated during the MD simulations, we assume that for a given residue, the carboxylic acid group (acting as the hydrogen bond donor D) can be H-bonded to acceptor A, which can be either an oxygen atom of the carbonyl amide (in the same residue or within

https://doi.org/10.1021/acs.biomac.1c00623
Biomacromolecules 2021, 22, 3543−3551

another residue) or to the carboxylic acid moiety of another residue.

For each donor/acceptor pair (i.e., residue 1−1, residue 1−2, residue 1−3, etc., see Figure S3), we measure the key geometrical parameters of the hydrogen bonds that are (i) the distance between the carboxylic acid hydroxyl oxygen atom and the amide oxygen atom or the closest oxygen from another carboxylic acid moiety, and (ii) the H-bond atomic triad angle. We consider a hydrogen bond to be effectively formed—by assigning a value of 1—if the distance is lower than 3.5 Å and if the angle is larger than 150°; otherwise a value of 0 is attributed to the considered H-bond donor/acceptor pair.[50] For each donor/acceptor pair, this measurement is done in every MD snapshot and summed (leading to a matrix of DP × DP). In Figure 3, we report these values for all H-bond donor/acceptor pairs averaged over the MD simulations, i.e., by dividing the total number computed for each donor−acceptor pair by the total number of generated structures. Such a representation allows to quickly visualize whether H-bonds are present as well as the residues involved. From these figures, we mainly detect non-null data along the diagonal, indicative that intraresidue H-bonds are increasingly formed along the peptoid backbone as the DP increases, except for a few residues lying at both the N and C termini, as nicely evidenced for DP 15. Inspection of the MD-generated structures, see Figure 2, reveals that few first residues at the N-terminus do not form H-bonds but have rather their amide oriented toward the ammonium group (Figure 2C, red dot box). As far as the C-terminal residue is concerned, the intraresidue H-bond is observed but in a different way than described above and is therefore not accounted for in Figure 3. It associates the hydrogen from the amide (acting now as a donor) and the carbonyl from the carboxylic acid group (acting as the acceptor, Figure 2C, green dot box, and see Figure S3 for a schematic explanation).

To estimate theoretically the minimum number of H-bonds required to stabilize a gaseous helix protruding out of the (charge solvation) loop, we first consider a model peptoid bearing methyl groups as pending side chains (*N*sar$_{5-7}$, Figure 4) to remove the contributions from the carboxylic acids in *N*scp peptoids and the phenyl groups in *N*spe. These model peptoids are built in a hypothetical right-handed helix, using the same dihedrals as described in references 18 and 34 that are similar to the poly(proline) type I helix. In parallel, we consider the loop structure obtained by a full conformational search (see Section 2).[34]

Using molecular mechanics, the energy difference between different conformations can be decomposed into different energetic contributions, i.e., the bonded (encompassing bond stretching, angle bending, dihedral, and improper dihedral) and the nonbonded (van der Waals, electrostatic, and hydrogen bonds, as implemented in the DREIDING force field[42]) interactions. The bonded and nonbonded energetic contributions have been extracted for each *N*sar model, in both the helical or loop conformations, and gathered in Table 1. For a given oligomer size, there are no major differences for the bonded energy contributions as well as for the hydrogen bond and van der Waals contributions between the helix and the corresponding loop. However, the electrostatic interactions differ significantly, with an average stabilization of about 15 kcal/mol in favor of loop conformations. In a very naive vision, secondary strong interactions, such as H-bonds, are thus

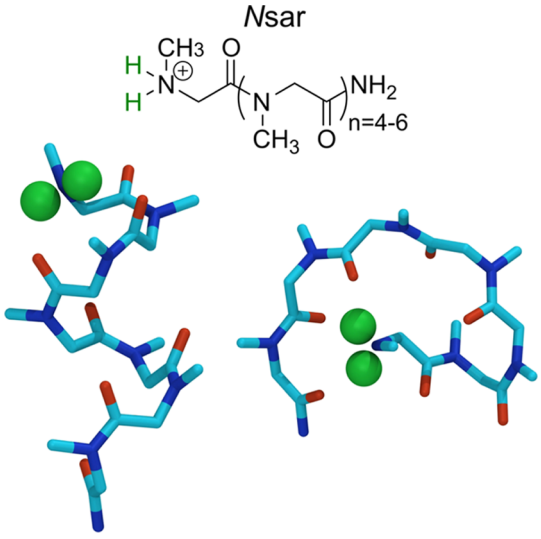

Figure 4. Primary structure of *N*sar peptoids and the hypothetic helical structure of *N*sar$_7$ and its associated loop structure (both protonated, as highlighted by green beads).

needed to compensate these 15 kcal/mol and make the helix conformations more stable than the loop structures.

Figure 5 presents the evolution of the hydrogen bond energy contribution of the *N*scp peptoids as a function of the degree of polymerization. The contributions are calculated for two geometries: (i) the perfect right-handed helix (blue dots) and (ii) the most stable structure obtained after the conformational sampling (black dots). The total H-bond energy is very similar in both cases, (blue and black dots), indicating that the H-bond pattern found in the most stable structure is similar in magnitude to that prevailing in the perfect helices. We have also extracted the H-bond contribution within the helical segment in the most stable structure, see Figure 5 (black crosses). To do so, for each chain length, we cut the most stable structure at the junction indicated by the hydrogen bond correlation matrices and performed a single point calculation on the segment that forms intraresidue hydrogen bonds (i.e., the helical segment), from which we extract the hydrogen bond energy contribution. Thereby we obtain three linear evolutions whose slopes afford an averaged stabilization energy per H-bond of around −2.5 kcal/mol. This value matches well that reported for α-helix (−2 kcal/mol),[51] allowing us to roughly estimate that a minimum of six or seven inter/intraresidue H-bonds should be enough to stabilize a charged helix in the gas phase. For the partially helical *N*scp$_8$ (Figure 2B), we clearly count four H-bonds between the side chain *i* and the backbone carbonyl *i*, starting at residue 4, as shown in Figure 3. The energetic gain provided by these four hydrogen bonds amounts to −10.8 kcal/mol (see Figure 5), which is close to the generic helix/loop difference estimated at 15 kcal/mol from the data in Table 1. *N*scp$_{15}$ clearly adopts a helical conformation stabilized by 10 H-bonds, as shown in Figure 3, hence leading to stabilization by −30 kcal/mol (Figure 5). Here, the H-bonds clearly prevent the peptoid ion from fully wrapping around the charge to form a compact structure. Actually, the ammonium group is still charge-solvated by the first three to four residues (see also Figure 3) but does not hamper the stabilization of a well-defined helical structure from the remaining units. Moreover, the charge is also stabilized by

https://doi.org/10.1021/acs.biomac.1c00623
Biomacromolecules 2021, 22, 3543−3551

Table 1. Energy Contributions (kcal/mol) Extracted from the Helical and Loop Structures from $Nsar_5$ to $Nsar_7$: Bonded Interactions, Hydrogen Bonds, Van der Waals (vdW) Interactions, and Electrostatic Interactions[a]

	helix				loop			
DP	bonded interactions	H-bonds	vdW	electrostatic	bonded interactions	H-bonds	vdW	electrostatic
5	25.4	−4.0	27.2	23.3	28.6	−4.3	24.5	11.5
6	30.7	−4.1	32.3	31.2	30.4	−5.9	32.9	16.9
7	36.0	−4.1	37.1	39.6	32.1	−3.2	37.6	25.1

[a]Larger differences are observed for the electrostatic interactions between the helical and loop shapes.

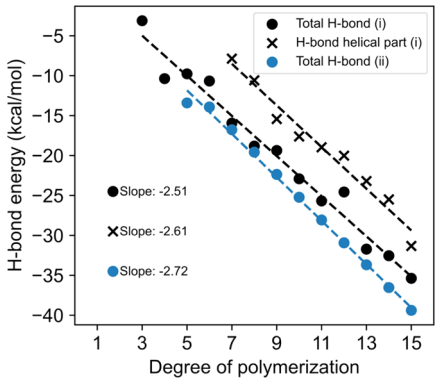

Figure 5. Evolution of the hydrogen bond energy contribution in the *N*scp peptoids as a function of the degree of polymerization. Contributions are calculated for two geometries: (i) the perfect right-handed helix (blue dots) and (ii) the most stable structure obtained upon conformational sampling (black dots). The H-bond contributions in the helical segments in the most stable structures (delimited by diagonal elements in Figure 3) are presented as black crosses.

the macrodipole formed by the alignment of the carbonyls from the C to the N-terminus.[18]

3.2. (*R*)-*N*-(1-Carboxy-2-ethyl) (*N*rce) Peptoids. Since bulky α-chiral side chains are described as a primary condition to stabilize helical peptoids in solution,[19,21] we further assess whether the H-bond capability of side chains is a sufficient condition to form helices in the gas phase. To do so, we select the *N*rce, (*R*)-*N*-(1-carboxy-2-ethyl), side chain (Scheme 1) that bears a methyl group instead of the phenyl group present in the *N*scp side chain. In this way, the α-chiral and H-bond donor/acceptor characters are conserved while partially releasing the steric hindrance via the elimination of the phenyl groups. We sample the conformational space of the *N*-protonated *N*rce peptoids (from DP 3 to 20) using the same method as for *N*scp peptoids. We compute the average $^{TM}\Omega_{He}$ for each chain length and report the CCS evolution as a function of mass in Figure 6 (blue dots). We also build model helices for each DP (using the same dihedrals as previously) and compute Ω_{He} for perfectly helical peptoids (Figure 6, blue dotted line). The curve (blue dots) built from the most stable structures starts to significantly deviate from the helical trend (black dashed line) at m/z 1200 (around 7 units). We have selected three representative chain lengths, DP = 5, 10, and 15, and displayed their most stable conformations in Figure 6. These ions are found to be very compact, i.e., they adopt a globular form, with the backbone wrapped around the charge (green beads), as observed in ref 38. When generating the hydrogen bond correlation matrices for these ions (Figure S4), we observe that intraresidue H-bonds are barely formed, while inter-residue H-bonds tend to be increasingly favored as the chain length increases. Finally, by plotting in Figure 6, the curve representing the standard CCS evolution of globular ions, i.e., $\Omega = 2.435\ M^{2/3}$,[38] we fully confirm that the *N*rce ions adopt compact structures in the gas phase, thus emphasizing that both the presence of H-bonds and the presence of bulky side chains are two key ingredients to stabilize peptoid helical ions in the gas phase.

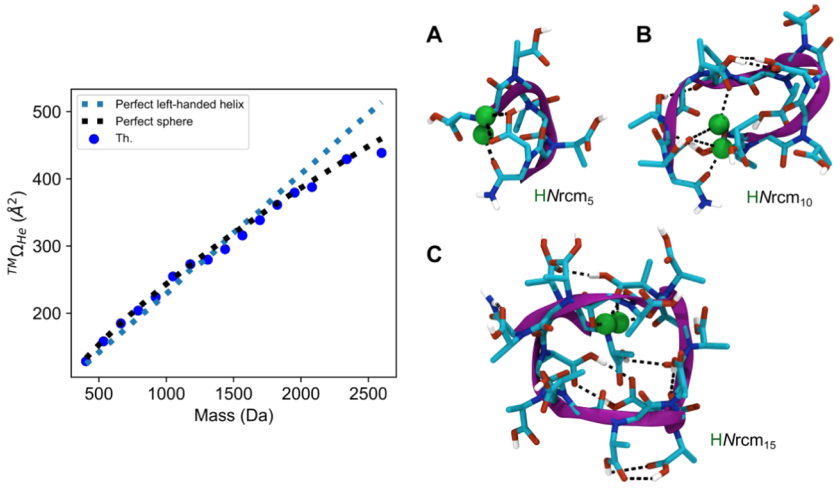

Figure 6. Theoretical collision cross sections (CCS) of protonated *N*rce peptoids. Comparison of the evolution of the theoretical CCS (Ω_{He}; blue dots) with the predicted data for perfectly spherical (black dashed line) and helical (blue dashed line) ions (see text). Optimized structures of protonated *N*rce (A) 5, (B) 10, and (C) 15 residues, revealing that the presence of H-bond donor/acceptor pairs along the peptoid backbone is not sufficient to stabilize helical conformations in the gas phase.

https://doi.org/10.1021/acs.biomac.1c00623
Biomacromolecules 2021, 22, 3543−3551

4. CONCLUSIONS

Numerous studies conducted in the condensed phase over the past 20 years reveal that different helical forms can be displayed by peptoid oligomers, thereby associating peptoids to foldamers. Nevertheless, these peptoid helical structures conform fairly closely to a canonical helical form due to extensive conformational dynamics, particularly including amide cis/trans isomerization processes. Mass spectrometry often proves to be a promising structural analysis method by capturing an instant picture of the peptoid conformational equilibrium by freezing the solution-phase structures upon transfer to the gas phase. Recent studies combined electrospray ionization and ion mobility mass spectrometry to prepare peptoid ions in the gas phase and study their conformations.[34] Interestingly, peptoids, known to be able to adopt helical structures in solution, were shown to adopt typically compact structures in the gas phase due to the charge solvation effects, i.e., the need to stabilize the charge introduced for the ionization process by intramolecular solvation. In such cases, the lack of strong secondary interactions such as intramolecular H-bonds prevents the ions to remain in their helical form. In the present work, we have incorporated H-bond donor groups all along the peptoid backbone as part of the pending side chains. Our joint experimental and theoretical study reveals that helical peptoid structures can now be detected in the gas phase primarily due to the formation of an intraresidue H-bond network associating the hydrogen atom from the side chain carboxylic acid to the oxygen atom of the amide inside the same residue. Finally, we demonstrated that the obtention of stable helical structures is conditioned by different factors: (i) the possibility to create intraresidue H-bonds, (ii) the presence of a sufficient amount of residues to energetically counterbalance the charge-induced folding (DP > 8), and (iii) the presence of bulky side chains to generate a high degree of steric hindrance.

■ ASSOCIATED CONTENT

Supporting Information

The Supporting Information is available free of charge at https://pubs.acs.org/doi/10.1021/acs.biomac.1c00623.

Further details about peptoid synthesis and characterization; ion mobility spectrometry protocols and additional data; force field parametrization; and molecular dynamics complementary analyses (PDF)

■ AUTHOR INFORMATION

Corresponding Authors

Jérôme Cornil − *Laboratory for Chemistry of Novel Materials, Center of Innovation and Research in Materials and Polymers (CIRMAP), University of Mons, UMONS, 7000 Mons, Belgium;* orcid.org/0000-0002-5479-4227; Email: Jerome.CORNIL@umons.ac.be

Pascal Gerbaux − *Organic Synthesis and Mass Spectrometry Laboratory, Center of Innovation and Research in Materials and Polymers (CIRMAP), University of Mons, UMONS, 7000 Mons, Belgium;* orcid.org/0000-0001-5114-4352; Email: Pascal.GERBAUX@umons.ac.be

Authors

Sébastien Hoyas − *Organic Synthesis and Mass Spectrometry Laboratory, Center of Innovation and Research in Materials and Polymers (CIRMAP), University of Mons, UMONS, 7000 Mons, Belgium; Laboratory for Chemistry of Novel Materials, Center of Innovation and Research in Materials and Polymers (CIRMAP), University of Mons, UMONS, 7000 Mons, Belgium*

Perrine Weber − *Organic Synthesis and Mass Spectrometry Laboratory, Center of Innovation and Research in Materials and Polymers (CIRMAP), University of Mons, UMONS, 7000 Mons, Belgium; Laboratory of Polymeric and Composite Materials, Center of Innovation and Research in Materials and Polymers (CIRMAP), University of Mons, UMONS, 7000 Mons, Belgium*

Emilie Halin − *Organic Synthesis and Mass Spectrometry Laboratory, Center of Innovation and Research in Materials and Polymers (CIRMAP), University of Mons, UMONS, 7000 Mons, Belgium*

Olivier Coulembier − *Laboratory of Polymeric and Composite Materials, Center of Innovation and Research in Materials and Polymers (CIRMAP), University of Mons, UMONS, 7000 Mons, Belgium;* orcid.org/0000-0001-5753-7851

Julien De Winter − *Organic Synthesis and Mass Spectrometry Laboratory, Center of Innovation and Research in Materials and Polymers (CIRMAP), University of Mons, UMONS, 7000 Mons, Belgium;* orcid.org/0000-0003-3429-5911

Complete contact information is available at: https://pubs.acs.org/10.1021/acs.biomac.1c00623

Author Contributions

S.H. and P.W. contributed equally to this research work. S.H. performed the calculations under the supervision of J.C. and P.W., and E.H. performed the experiments under the supervision of J.D.W., O.C., and P.G. All authors have contributed to the writing of the manuscript and given their approval to the final version.

Notes

The authors declare no competing financial interest.

■ ACKNOWLEDGMENTS

The work in the Laboratory for Chemistry of Novel Materials was supported by the Consortium des 'Equipements de Calcul Intensif' funded by the Fonds National de la Recherche Scientifique (FRS-FNRS) under Grant No. 2.5020.11. The S^2MOs lab is grateful to the FRS-FNRS for financial support in the acquisition of the Waters Synapt G2-S*i* mass spectrometer. J.C., O.C., and P.W. are FNRS research fellows. S.H. thanks the "Fonds pour la Recherche Industrielle et Agricole" for his Ph.D. grant.

■ REFERENCES

(1) Sanford, A.; Gong, B. Evolution of Helical Foldamers. *Curr. Org. Chem.* **2003**, *7*, 1649−1659.

(2) Guichard, G.; Huc, I. Synthetic Foldamers. *Chem. Commun.* **2011**, *47*, 5933−5941.

(3) Nizami, B.; Bereczki-Szakál, D.; Varró, N.; El Battioui, K.; Nagaraj, V. U.; Szigyártó, I. C.; Mándity, I.; Beke-Somfai, T. FoldamerDB: A Database of Peptidic Foldamers. *Nucleic Acids Res.* **2020**, *48*, D1122−D1128.

(4) Seebach, D.; Beck, A. K.; Bierbaum, D. J. The World of β- And γ-Peptides Comprised of Homologated Proteinogenic Amino Acids and Other Components. *Chem. Biodiversity* **2004**, *1*, 1111−1239.

(5) Fischer, L.; Claudon, P.; Pendem, N.; Miclet, E.; Didierjean, C.; Ennifar, E.; Guichard, G. The Canonical Helix of Urea Oligomers at

Atomic Resolution: Insights Into Folding-Induced Axial Organization. *Angew. Chem., Int. Ed.* **2010**, *49*, 1067−1070.
(6) Wu, C. W.; Kirshenbaum, K.; Sanborn, T. J.; Patch, Ja.; Huang, K.; Dill, K.; Zuckermann, R. N.; Barron, A. E. Structural and Spectroscopic Studies of Peptoid Oligomers with α-Chiral Aliphatic Side Chains. *J. Am. Chem. Soc.* **2003**, *125*, 13525−13530.
(7) Ganesh, S. D.; Saha, N.; Zandraa, O.; Zuckermann, R. N.; Sáha, P. Peptoids and Polypeptoids: Biomimetic and Bioinspired Materials for Biomedical Applications. *Polym. Bull.* **2017**, *74*, 3455−3466.
(8) Zuckermann, R. N.; Kerr, J. M.; Kent, S. B. H.; Moos, W. H. Efficient Method for the Preparation of Peptoids [Oligo(N-Substituted Glycines)] by Submonomer Solid-Phase Synthesis. *J. Am. Chem. Soc.* **1992**, *114*, 10646−10647.
(9) Miller, S. M.; Simon, R. J.; Ng, S.; Zuckermann, R. N.; Kerr, J. M.; Moos, W. H. Proteolytic Studies of Homologous Peptide and N-Substituted Glycine Peptoid Oligomers. *Bioorg. Med. Chem. Lett.* **1994**, *4*, 2657−2662.
(10) Sanborn, T. J.; Wu, C. W.; Zuckermann, R. N.; Barron, A. E. Extreme Stability of Helices Formed by Water-Soluble Poly-N-Substituted Glycines (Polypeptoids) with α -Chiral Side Chains. *Biopolymers* **2002**, *63*, 12−20.
(11) Chongsiriwatana, N. P.; Patch, J. A.; Czyzewski, A. M.; Dohm, M. T.; Ivankin, A.; Gidalevitz, D.; Zuckermann, R. N.; Barron, A. E. Peptoids That Mimic the Structure, Function, and Mechanism of Helical Antimicrobial Peptides. *Proc. Natl. Acad. Sci. U.S.A.* **2008**, *105*, 2794−2799.
(12) Fowler, Sa.; Blackwell, H. E. Structure-Function Relationships in Peptoids: Recent Advances toward Deciphering the Structural Requirements for Biological Function. *Org. Biomol. Chem.* **2009**, *7*, 1508−1524.
(13) Sun, J.; Li, Z. Peptoid Applications in Biomedicine and Nanotechnology. In *Peptide Applications in Biomedicine, Biotechnology and Bioengineering*; Elsevier, 2018; pp 183−213.
(14) Olivier, G. K.; Cho, A.; Sanii, B.; Connolly, M. D.; Tran, H.; Zuckermann, R. N. Antibody-Mimetic Peptoid Nanosheets for Molecular Recognition. *ACS Nano* **2013**, *7*, 9276−9286.
(15) Statz, A. R.; Meagher, R. J.; Barron, A. E.; Messersmith, P. B. New Peptidomimetic Polymers for Antifouling Surfaces. *J. Am. Chem. Soc.* **2005**, *127*, 7972−7973.
(16) Lau, K. H. A.; Ren, C.; Sileika, T. S.; Park, S. H.; Szleifer, I.; Messersmith, P. B. Surface-Grafted Polysarcosine as a Peptoid Antifouling Polymer Brush. *Langmuir* **2012**, *28*, 16099−16107.
(17) Nam, K. T.; Shelby, Sa.; Choi, P. H.; Marciel, A. B.; Chen, R.; Tan, L.; Chu, T. K.; Mesch, R.; Lee, B.-C.; Connolly, M. D.; Kisielowski, C.; Zuckermann, R. N. Free-Floating Ultrathin Two-Dimensional Crystals from Sequence-Specific Peptoid Polymers. *Nat. Mater.* **2010**, *9*, 454−460.
(18) Armand, P.; Kirshenbaum, K.; Falicov, A.; Dunbrack, R. L.; Dill, K.; Zuckermann, R. N.; Cohen, F. E. Chiral N-Substituted Glycines Can Form Stable Helical Conformations. *Folding Des.* **1997**, *2*, 369−375.
(19) Wu, C. W.; Sanborn, T. J.; Huang, K.; Zuckermann, R. N.; Barron, A. E. Peptoid Oligomers with α-Chiral, Aromatic Side Chains: Sequence Requirements for the Formation of Stable Peptoid Helices. *J. Am. Chem. Soc.* **2001**, *123*, 6778−6784.
(20) John, E. A.; Massena, C. J.; Berryman, O. B. Helical Anion Foldamers in Solution. *Chem. Rev.* **2020**, *120*, 2759−2782.
(21) Wu, C. W.; Sanborn, T. J.; Zuckermann, R. N.; Barron, A. E. Peptoid Oligomers with α-Chiral, Aromatic Side Chains: Effects of Chain Length on Secondary Structure. *J. Am. Chem. Soc.* **2001**, *123*, 2958−2963.
(22) Gorske, B. C.; Nelson, R. C.; Bowden, Z. S.; Kufe, T. A.; Childs, A. M. "Bridged" n →π* Interactions Can Stabilize Peptoid Helices. *J. Org. Chem.* **2013**, *78*, 11172−11183.
(23) Hudgins, R. R.; Ratner, M. A.; Jarrold, M. F. Design of Helices That Are Stable in Vacuo. *J. Am. Chem. Soc.* **1998**, *120*, 12974−12975.
(24) Hudgins, R. R.; Jarrold, M. F. Helix Formation in Unsolvated Alanine-Based Peptides: Helical Monomers and Helical Dimers. *J. Am. Chem. Soc.* **1999**, *121*, 3494−3501.
(25) Hudgins, R.; Jarrold, M. Conformations of Unsolvated Glycine-Based Peptides. *J. Phys. Chem. B* **2000**, *104*, 2154−2158.
(26) Lanucara, F.; Holman, S. W.; Gray, C. J.; Eyers, C. E. The Power of Ion Mobility-Mass Spectrometry for Structural Characterization and the Study of Conformational Dynamics. *Nat. Chem.* **2014**, *6*, 281−294.
(27) Gabelica, V.; Marklund, E. Fundamentals of Ion Mobility Spectrometry. *Curr. Opin. Chem. Biol.* **2018**, *42*, 51−59.
(28) Gabelica, V.; Shvartsburg, A. A.; Afonso, C.; Barran, P.; Benesch, J. L. P.; Bleiholder, C.; Bowers, M. T.; Bilbao, A.; Bush, M. F.; Campbell, J. L.; Campuzano, I. D. G.; Causon, T.; Clowers, B. H.; Creaser, C. S.; De Pauw, E.; Far, J.; Fernandez-Lima, F.; Fjeldsted, J. C.; Giles, K.; Groessl, M.; Hogan, C. J.; Hann, S.; Kim, H. I.; Kurulugama, R. T.; May, J. C.; McLean, J. A.; Pagel, K.; Richardson, K.; Ridgeway, M. E.; Rosu, F.; Sobott, F.; Thalassinos, K.; Valentine, S. J.; Wyttenbach, T. Recommendations for Reporting Ion Mobility Mass Spectrometry Measurements. *Mass Spectrom. Rev.* **2019**, *38*, 291−320.
(29) Uetrecht, C.; Rose, R. J.; van Duijn, E.; Lorenzen, K.; Heck, A. J. R. Ion Mobility Mass Spectrometry of Proteins and Protein Assemblies. *Chem. Soc. Rev.* **2010**, *39*, 1633−1655.
(30) Ben-Nissan, G.; Sharon, M. The Application of Ion-Mobility Mass Spectrometry for Structure/Function Investigation of Protein Complexes. *Curr. Opin. Chem. Biol.* **2018**, *42*, 25−33.
(31) Hoskins, J. N.; Trimpin, S.; Grayson, S. M. Architectural Differentiation of Linear and Cyclic Polymeric Isomers by Ion Mobility Spectrometry-Mass Spectrometry. *Macromolecules* **2011**, *44*, 6915−6918.
(32) Liénard, R.; Duez, Q.; Grayson, S. M.; Gerbaux, P.; Coulembier, O.; De Winter, J. Limitations of Ion Mobility Spectrometry-mass Spectrometry for the Relative Quantification of Architectural Isomeric Polymers: A Case Study. *Rapid Commun. Mass Spectrom.* **2020**, *34*, 1−11.
(33) Hudgins, R. R.; Mao, Y.; Ratner, M.; Jarrold, M. F. Conformations of GlynH+ and AlanH+ Peptides in the Gas Phase. *Biophys. J.* **1999**, *76*, 1591−1597.
(34) Hoyas, S.; Halin, E.; Lemaur, V.; De Winter, J.; Gerbaux, P.; Cornil, J. Helicity of Peptoid Ions in the Gas Phase. *Biomacromolecules* **2020**, *21*, 903−909.
(35) Taraszka, J. A.; Counterman, A. E.; Clemmer, D. E. Large Anhydrous Polyalanine Ions: Substitution of Na+ for H+ Destabilizes Folded States. *Int. J. Mass Spectrom.* **2001**, *204*, 87−100.
(36) Shin, S. B. Y.; Kirshenbaum, K. Conformational Rearrangements by Water-Soluble Peptoid Foldamers. *Org. Lett.* **2007**, *9*, 5003−5006.
(37) Tran, H.; Gael, S. L.; Connolly, M. D.; Zuckermann, R. N. Solid-Phase Submonomer Synthesis of Peptoid Polymers and Their Self-Assembly into Highly-Ordered Nanosheets. *J. Visualized Exp.* **2011**, No. 3373.
(38) Ruotolo, B. T.; Benesch, J. L. P.; Sandercock, A. M.; Hyung, S.-J.; Robinson, C. V. Ion Mobility−Mass Spectrometry Analysis of Large Protein Complexes. *Nat. Protoc.* **2008**, *3*, 1139−1152.
(39) Duez, Q.; Chirot, F.; Liénard, R.; Josse, T.; Choi, C.; Coulembier, O.; Dugourd, P.; Cornil, J.; Gerbaux, P.; De Winter, J. Polymers for Traveling Wave Ion Mobility Spectrometry Calibration. *J. Am. Soc. Mass Spectrom.* **2017**, *28*, 2483−2491.
(40) *Dassault Systèmes BIOVIA, Materials Studio, 18.0*; Dassault Systèmes: San Diego, 2018.
(41) Hoyas, S.; Lemaur, V.; Duez, Q.; Saintmont, F.; Halin, E.; De Winter, J.; Gerbaux, P.; Cornil, J. PEPDROID: Development of a Generic DREIDING-Based Force Field for the Assessment of Peptoid Secondary Structures. *Adv. Theory Simul.* **2018**, *1*, No. 1800089.
(42) Mayo, S. L.; Olafson, B. D.; Goddard, W. A. DREIDING: A Generic Force Field for Molecular Simulations. *J. Phys. Chem. A* **1990**, *94*, 8897−8909.
(43) Gasteiger, J.; Marsili, M. A New Model for Calculating Atomic Charges in Molecules. *Tetrahedron Lett.* **1978**, *19*, 3181−3184.
(44) Frisch, M. J.; Trucks, G. W.; Schlegel, H. B.; Scuseria, G. E.; Robb, M. A.; Cheeseman, J. R.; Scalmani, G.; Barone, V.; Petersson,

https://doi.org/10.1021/acs.biomac.1c00623
Biomacromolecules 2021, 22, 3543−3551

G. A.; Nakatsuji, H.; Li, X.; Caricato, M.; Marenich, A.; Bloino, J.; Janesko, B. G.; Gomperts, R.; Mennucci, B.; Hratchian, H. P.; Ort, J. V.; D, J. F. *Gaussian 09*, Revision A.02

(45) Ewing, S. A.; Donor, M. T.; Wilson, J. W.; Prell, J. S. Collidoscope: An Improved Tool for Computing Collisional Cross-Sections with the Trajectory Method. *J. Am. Soc. Mass Spectrom.* **2017**, *28*, 587−596.

(46) Halin, E.; Hoyas, S.; Lemaur, V.; De Winter, J.; Laurent, S.; Connolly, M. D.; Zuckermann, R. N.; Cornil, J.; Gerbaux, P. Backbone Cleavages of Protonated Peptoids upon Collision-Induced Dissociation: Competitive and Consecutive B-Y and A1-YX Reactions. *J. Am. Soc. Mass Spectrom.* **2019**, *30*, 2726−2740.

(47) Duez, Q.; Josse, T.; Lemaur, V.; Chirot, F.; Choi, C. M.; Dubois, P.; Dugourd, P.; Cornil, J.; Gerbaux, P.; De Winter, J. Correlation between the Shape of the Ion Mobility Signals and the Stepwise Folding Process of Polylactide Ions. *J. Mass Spectrom.* **2017**, *52*, 133−138.

(48) Saintmont, F.; De Winter, J.; Chirot, F.; Halin, E.; Dugourd, P.; Brocorens, P.; Gerbaux, P. How Spherical Are Gaseous Low Charged Dendrimer Ions: A Molecular Dynamics/Ion Mobility Study? *J. Am. Soc. Mass Spectrom.* **2020**, *31*, 1673−1683.

(49) De Winter, J.; Lemaur, V.; Ballivian, R.; Chirot, F.; Coulembier, O.; Antoine, R.; Lemoine, J.; Cornil, J.; Dubois, P.; Dugourd, P.; Gerbaux, P. Size Dependence of the Folding of Multiply Charged Sodium Cationized Polylactides Revealed by Ion Mobility Mass Spectrometry and Molecular Modelling. *Chem. - Eur. J.* **2011**, *17*, 9738−9745.

(50) Van Der Spoel, D.; Van Maaren, P. J.; Larsson, P.; Tîmneanu, N. Thermodynamics of Hydrogen Bonding in Hydrophilic and Hydrophobic Media. *J. Phys. Chem. B* **2006**, *110*, 4393−4398.

(51) Sheu, S. Y.; Yang, D. Y.; Selzle, H. L.; Schlag, E. W. Energetics of Hydrogen Bonds in Peptides. *Proc. Natl. Acad. Sci. U.S.A.* **2003**, *100*, 12683−12687.

https://doi.org/10.1021/acs.biomac.1c00623
Biomacromolecules 2021, 22, 3543−3551